Mass movement within a slope streak on Mars

Cynthia B. Phillips,[1] Devon M. Burr,[1] and Ross A. Beyer[1,2]

Received 6 August 2007; revised 25 September 2007; accepted 8 October 2007; published 6 November 2007.

[1] Slope streaks on Mars represent a currently active geological process. Various theories for slope streak formation have suggested that slope streaks form by disturbing only a thin surface veneer, or by staining of the surface, preserving pre-existing topography within the streak. Theories also vary as to whether the formation mechanism requires the presence of water or another liquid. We present observations of a slope streak that reveal topographic mounds within the streak. These mounds do not continue outside the streak, and we suggest that they formed with, or immediately after, the slope streak. We use estimates of the total volume of mounds in this particular streak, compared with the estimated excavation volume, to extrapolate to a global sediment transport rate from slope streak formation. If this slope streak is typical, then this calculated rate is greater than estimates of the total volume of material transported by dust storms each year. **Citation:** Phillips, C. B., D. M. Burr, and R. A. Beyer (2007), Mass movement within a slope streak on Mars, *Geophys. Res. Lett.*, *34*, L21202, doi:10.1029/2007GL031577.

1. Introduction

[2] Slope streaks on Mars are enigmatic features first observed by the Viking Orbiters [*Morris*, 1982], and later at higher resolutions by the Mars Orbiter Camera (MOC) on the Mars Global Surveyor (MGS) spacecraft [*Malin and Edgett*, 2001; *Sullivan et al.*, 2001]. In plan view, slope streaks have fan-shaped morphologies with an assumed origin at a point source. They often have wedge-shaped, branching, or braided patterns downslope. In previous data, the streaks showed no discernable topographic relief and did not have debris at their distal ends. Streaks also seemed to preserve the texture and roughness of the underlying surface without distortion [*Miyamoto et al.*, 2004], and are strongly correlated with regions of low thermal inertia [*Sullivan et al.*, 2001; *Schorghofer et al.*, 2002; *Chuang et al.*, 2007]. On the basis of these observed morphologies, two types of models have been proposed: (1) dry mass movement in the form of dust avalanches [*Morris*, 1982; *Williams*, 1991; *Sullivan et al.*, 2001; *Baratoux et al.*, 2006] and (2) wet liquid flow that transports, lubricates or stains the surface material [*Ferguson and Lucchitta*, 1984; *Ferris et al.*, 2002; *Head et al.*, 2007].

[3] This work presents new observations made of a wishbone-shaped dark slope streak by the Mars Global Surveyor (MGS) Mars Orbital Camera (MOC) at near full resolution, and more recently by the Mars Reconnaissance Orbiter (MRO) High Resolution Imaging Science Experiment (HiRISE [*McEwen et al.*, 2007]) camera. Quantitative analysis of the MOC image, along with qualitative confirmation from the HiRISE image, shows meter-scale topography within the low albedo area denoting the slope streak. This topography is not present outside the slope streak. We interpret these observations as indicating that slope streak formation entailed or caused significant sediment movement and is not simply a surface staining process. To the degree that this slope streak is typical on Mars [*Chuang et al.*, 2007], the evidence of topography puts constraints on the slope streak formation mechanism and provides data for estimating contemporary sediment volume fluxes resulting from slope streak formation. These estimates can then be compared with other sediment transport mechanisms currently operating on the surface of Mars.

2. Photoclinometry and Slope Streak Morphology

[4] MOC image R09/00701 (1.51 m/pixel) shows a 2.75-km-long slope streak (Figure 1) located on the northern scarp of Olympus Mons, a region of late Amazonian lava flows [*Scott and Tanaka*, 1986] and/or glacial activity within the last 100 Ma [*Neukum et al.*, 2004]. Individual tracks from Mars Orbiter Laser Altimeter (MOLA) data along the slope streak path have a slope range of 11–22 degrees [*Smith et al.*, 1999]. Numerous dust devil tracks and low Thermal Emission Spectrometer (TES) thermal inertia values [*Putzig et al.*, 2005] indicate that the region is covered by dust.

[5] For the purposes of our analyses, the streak can be divided into two sections, upslope and downslope. In the upslope section, it spreads outward from its origination point for $\sim$1.4 km, reaching a maximum width of $\sim$0.3 km. The downslope section begins at the point where the streak bifurcates, most likely due to a 5–10 m-high ridge. The streak continues down the slope forming distinct eastern and western branches (Figure 1). The MOC image shows a few dozen linear mounds in the low-albedo area covered by the streak. The mounds occur preferentially in the distal ends of both the upslope and downslope sections (Figures 1 and 2), and were first noted by *Verba and Phillips* [2006]. Such distinct mounds do not occur outside of the dark-toned area of the streak.

[6] Roughness analysis using point photoclinometry shows that the RMS slopes of various sample areas outside the low-albedo slope streak area are lower than for areas with mounds within the slope streak (Table 1). Photoclinometry, or shape-from-shading, assumes a flat surface with a uniform albedo in order to derive topographic information from variations in brightness [*Beyer et al.*, 2003]. The slope streak itself is on a gradual slope, but a boxcar filtering method [*Beyer et al.*, 2003] was used to minimize the effect of the long-wavelength slopes and allow

[1] Carl Sagan Center for the Study of Life in the Universe, SETI Institute, Mountain View, California, USA.
[2] NASA Ames Research Center, Moffett Field, California, USA.

0094-8276/07/2007GL031577$05.00

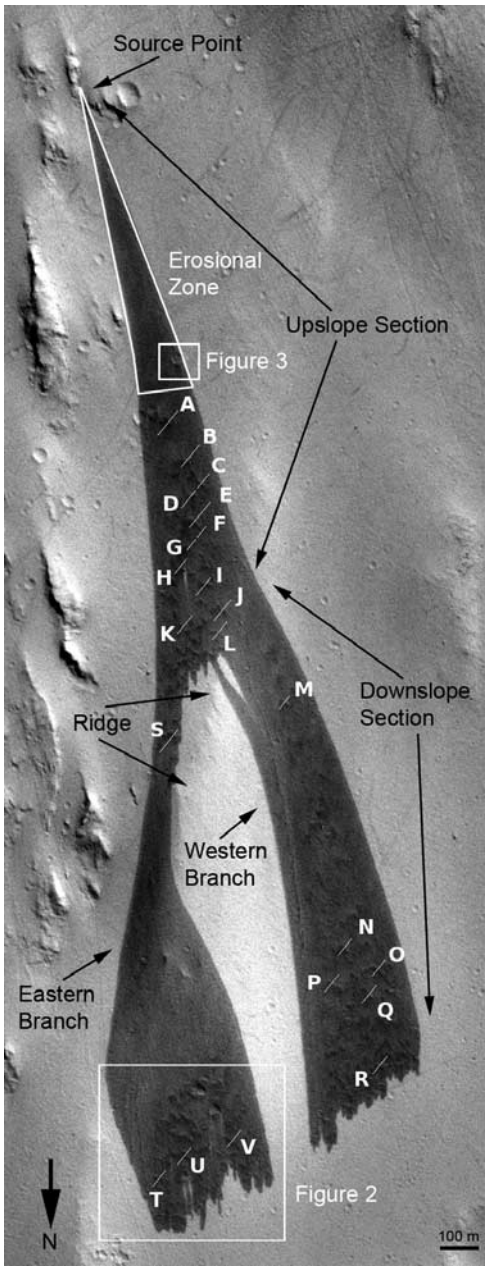

Figure 1. Portion of MOC image R09/00701 (1.5 m/pixel) showing dark slope streak with locations of photoclinometric profiles (see Table 2 for height measurements), and outlines of the areas shown in Figures 2 and 3. The sun is from the upper right, and north is down.

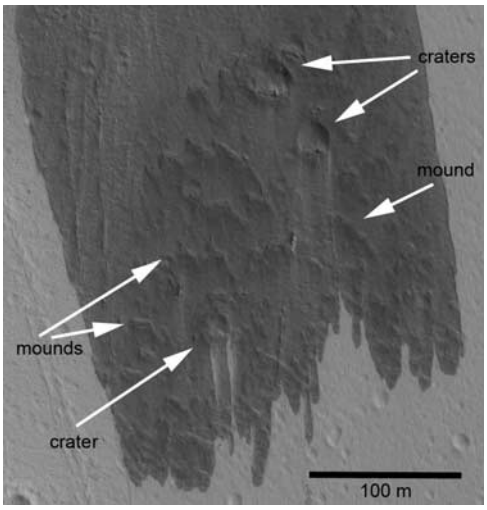

Figure 2. Portion of HiRISE image PSP_003542_2035. Distal end of the slope streak's eastern branch showing several linear mounds, interpreted to have formed in association with the slope streak, and eroded craters, interpreted as existing prior to slope streak formation. The sun is from the right, and north is down.

analysis of the shorter-wavelength slopes of interest in this study, effectively eliminating the 11–22 degree regional slopes from the measurements. The photoclinometry data show a difference in roughness between the slope streak and non-slope streak areas. We infer that the greater roughness within the slope streak, caused by the formation of linear mounds, is confined to the slope streak, and therefore that the mounds are a result of slope streak formation.

[7] These linear mounds occur preferentially at the distal ends of both the upslope and downslope sections of the streak. The accumulations of material at the distal ends of each section suggest transport of material down the Olympus Mons scarp from the proximal (i.e., upper) parts of each section. In order to assess the amount of material in these mounds, we performed profile photoclinometry measurements across 22 mounds in the MOC image (Figure 1).

[8] Our results show that the heights of mounds range from about 1 meter to 5 meters (Table 2). Mound shapes were generally symmetric, to within the errors of the photoclinometry technique. Heights were measured at the central or most prominent portion of each mound, and/or at a location that was favorable for the placement of a photoclinometry profile (e.g., having strong topographic shading, a flat surface surrounding the mound, etc).

3. Sediment Transport

[9] We used the mound heights to estimate the total amount of sediment transported by the formation of this streak. This approach assumes that no material has been lost from the mounds from erosion subsequent to formation, so is an underestimate of sediment transport; we consider other sources of errors later in this section. We measured the

Table 1. Statistics for Average Surface Slope Both Within and Outside the Slope Streak[a]

Location	Ave. Slope, °	RMS Dev., °
All material outside streak	0.36	5.41
Nearby material outside streak (w/o ridges)	0.24	3.89
All material inside streak	0.62	8.03

[a]Slope measurements in areas slightly outside the streak, without ridges, represent the type of material covered by the slope. Ave. Slope is the average slope value (in degrees), and RMS Dev = $\sqrt{\sum_i (i-\bar{i})^2} \Big/ n-1$, where i is each slope (pixel) in the sample and n is the number of slopes. The results show a difference in the average slope and in the RMS deviation inside and outside the streak, indicating that the streak has a rougher texture than surrounding materials.

Table 2. Volumes of Mounds and Source Regions, and the Cumulative Total Over the Entire MOC Image

Profile	Height, m	Width, m	Length, m	Volume, m^3
A	4.6	15	35	1208
B	4.4	8	31	546
C	4.9	17	30	1250
D	4.5	17	23	880
E	3.1	30	53	2465
F	2.1	7	11	81
G	2.1	22	38	878
H	1.6	11	21	185
I	1.8	18	36	583
J	2.9	14	30	609
K	2.9	14	71	1441
L	2.3	17	50	978
M	2.4	11	34	449
N	3.3	20	53	1749
O	2.1	20	63	1323
P	1	17	51	434
Q	2.8	26	49	1784
R	0.8	12	35	168
S	2.6	17	29	641
T	0.8	13	39	203
U	1.8	14	51	643
V	3.7	16	62	1835
Total volume				20329
Source Region	1	120	800	48000

length and width of the mounds as seen in planview and assumed a triangular cross-section to estimate the total volume of each mound. Mound lengths varied from 10–70 meters, with widths of 7–30 meters (Table 2). We estimate a minimum volume of about 20,000 m^3 for the total amount of material contained in the 22 measured mounds. This approach overestimates the volume of each individual mound because only the most prominent and therefore likely highest parts of the mounds were measured, and the mound height must decrease at the ends of the mounds.

[10] The estimate of a triangular cross section may lead to an underestimate of the total volume of each mound if the cross section is in fact concave upwards and the mounds have more of a dome shape. However, we only measured the most obvious mounds in the MOC image, so our result underestimates the total volume of material in the mounds. A HiRISE image covering the same area, image PSP_003542_2035, shows many additional mounds at a resolution of 25 cm/pixel. Quantitative analysis of the HiRISE image awaits radiometric and geometric image calibration, and our total volume estimate above should be treated as a lower limit.

[11] The total volume of sediment deposited at the distal ends of both the upper and lower sections appears consistent with the total volume of sediment eroded and/or entrained at the proximal end of the upslope section. In the HiRISE image, the edges of the slope streak at these locations (Figure 3) show topographic shading, implying a slight step-down from the surroundings to the interior of the slope streak. This elevation difference is not visible in the MOC image, and so must be less than 1 meter (below the limit of MOC resolution), given the solar azimuth and spatial resolution of the MOC image (consistent with *Chuang et al.* [2007]). The presence of a region of excavation is similar to that observed by *Gerstell et al.* [2004] and interpreted as avalanche scarring, although those authors measured depths on the order of several meters.

[12] A maximum elevation difference of ~1 m over the proximal portion of the upper section equates to a maximum volume of ~50,000 m^3 removed from the erosional zone (Figure 1, Table 2). This is greater than the measured minimum volume of material in the mounds at the distal ends of the upper and lower sections of 20,000 m^3. Given the likelihood of dust compaction, loss of material to the atmosphere during transport, and error in these low resolution measurements, these comparisons are consistent with the hypothesis of dark slope streak formation through sediment entrainment in the proximal portion of the streak and sediment deposition in the distal portions. The HiRISE image reveals that a more subtle scarp extends almost to the end of the distal portion of the slope (Figure 2), interrupted by positive relief mounds. It is possible to have erosion continuing at the lateral margins of the streak while deposition takes place in the interior.

4. Implications

[13] Our mass transport estimates for this dark slope streak have several implications regarding slope streak formation and associated processes on Mars. First, the proposed mechanisms that rely solely on staining of the surface for the observed slope streak albedo [*Ferris et al.*, 2002; *Head et al.*, 2007] are not consistent with a material removal process as shown from our analysis. Either the staining mechanism does not provide a fully sufficient explanation for the formation of slope streaks, or slope streaks are formed by multiple mechanisms.

[14] Second, dark slope streaks represent one of the most dynamic geological processes currently altering the Martian

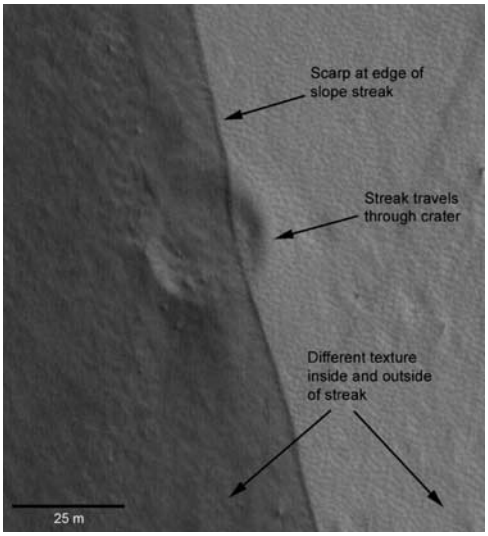

Figure 3. Portion of HiRISE image PSP_003542_2035, showing a change in elevation (depression) over the proximal part of the upslope section, suggesting that this is a zone of erosion. A textural difference between the material inside and outside of the streak is also apparent (see Table 1). Note that the streak travels through a small crater with little or no diversion. The sun is from the right, and North is down.

surface. *Aharonson et al.* [2003] estimated that as many as 800,000 slope streaks could exist on Mars in regions with low thermal inertia, which cover 2.3×10^7 km^2 or about 16% of the surface area of Mars. *Schorghofer et al.* [2007] estimate that new slope streaks form at a rate of 0.03 streaks per existing streak per year. For a total of 800,000 slope streaks, this is approximately 24,000 new streaks formed per year. Thus, the minimum sediment movement in this slope streak (if typical), as implied by the observed topography, would equate to a minimum of 5×10^8 m^3 of sediment transport per year associated with slope streak formation.

[15] These volume estimates makes slope streak formation a potentially significant process when compared with other sediment transport processes currently operating on Mars [*Malin et al.*, 2006]. Global rates of sediment transport from gully formation and impact cratering are poorly constrained, but estimates for global aeolian dust transport are available. Comparison of Viking and Mariner 9 images with MGS images indicates that a total area of 56 million km^2 changed albedo by more than 10% during the 20 years between these missions [*Geissler*, 2005]. If we assume that a 10% albedo change requires the addition or removal of approximately 20 μm of dust, this implies that $\sim 10^7$ m^3 of dust was moved during this time, or about 0.5 million m^3 of dust per year. This value is three orders of magnitude less than the volumetric estimates for dust movement during slope streak formation. However, this is likely a minimum value, as dust may be transported without surface albedo change.

[16] Another estimate of global dust transport comes from global atmospheric dust models. *Cantor et al.* [2001] estimated the global dust loading in the atmosphere for the year 1999, based on orbital observations of dust storms. They estimate that 5×10^8 metric tons were transported by local and regional dust storms during that one year period. Assuming a typical dust density of 3000 kg/m^3 and that this transport rate is an average one, this would equal a sediment transport rate of 1.7×10^8 m^3 per year from global dust storms. This is of the same order of magnitude as our estimate of 5×10^8 m^3 of surface sediment transport per year from slope streak formation. Even if this streak is larger than average, a factor of 5 reduction in area still results in a sediment transport rate comparable to that by global dust storms. Processes like these likely redistribute dust transported in the formation of slope streaks, removing them from view and priming the surface for the formation of future streaks.

5. Summary and Conclusions

[17] The largest slope streak shown in MOC image R09-00701 and subsequent HiRISE image PSP_003542_2035 has many linear mounds with maximum heights of a few meters. This topographic expression is confined to the streak, indicating that its creation was associated with steak formation. This creation may have occurred either during slope streak formation or subsequent to it. Subsequent formation may occur, for example, by slumping because of sediment destabilization, although no noticeable excavation immediately upslope of individual mounds, as would be expected from slumping, is apparent in our photoclinometry profiles. The total volume of material contained in these mounds is a minimum of $\sim$20,000 m^3, whereas the total volume of material removed from upslope of the mounds is $\sim$50,000 m^3.

[18] These values suggest formation of the mounds by erosion, transport in the downslope direction, and deposition of sediment within the streak. This is consistent with the hypothesis of slope streak formation by dust avalanches [*Sullivan et al.*, 2001; *Baratoux et al.*, 2006; *Chuang et al.*, 2007], but does not rule out an aqueous process. In this particular case, the slope is less than the angle of repose, possibly adding support to a model in which water has some sort of lubricating role [*Ferguson and Lucchitta*, 1984; *Ferris et al.*, 2002; *Head et al.*, 2007].

[19] In support of our sediment transport hypothesis, the relative locations of the linear mounds suggest that transport was influenced by underlying slopes. Deposition of material from a flow occurs when the flow velocity drops below some threshold value, usually related to particle settling velocity [e.g., *Rouse*, 1937]. Because more shallow slopes reduce flow velocity, they commonly result in sediment deposition, as discussed by *Sullivan et al.* [2001]. This relationship between slope and deposition is observed in the slope streak discussed here. In Figure 1, the deposition of material in linear mounds first occurs immediately upslope of the pre-existing ridge. This location suggests that the ridge caused a reduction of the flow velocity that was sufficient to produce sediment deposition. The lateral eastward shift of the slope streak's eastern branch shows that the ridge was also sufficient to divert material movement. In the lower section of both the eastern and western branches, the mounds are again located at the distal ends. This deposition of material suggests that the flow was decreasing in velocity to initiate deposition, perhaps due to a decrease in slope or a decrease in an initial energy input (i.e., from a possible energetic origination). Thus, the relative locations of the linear mounds support their formation by deposition out of a sediment-laden flow, due to a reduction in flow velocity.

[20] The appearance of the mounds and the streak itself is also consistent with streak formation by a sediment-laden flow. The sharp but localized relief of the mounds and their jagged planview shape give an appearance of cohesion to the mounds (e.g., Figure 2) similar to that of mudflows on Earth, in which clay-sized particles can produce internal strength. However, these observations can not discriminate between the hypotheses of sediment transport by either flowing liquid (i.e. a mudflow) or flowing gas (i.e. a dust avalanche).

[21] Future studies of slope streak images from the MOC and HiRISE cameras will reveal whether the topography described in this work is typical of other slope streaks. To date, HiRISE images have shown that many slope streaks are depressed below the surrounding terrain, but associated distal deposits may be rare [*Chuang et al.*, 2007]. If this streak is unlike most other observed slope streaks, multiple formation mechanisms may be required to explain the diversity of morphologies.

[22] **Acknowledgments.** CBP and DMB were supported by the NASA Mars Data Analysis Program. RAB was supported by the MRO Participating Scientist Program. Initial observations of this feature were made by Circe Verba, who was supported by NSF REU grant AST-0552751. We also thank Frank Chuang, Paul Geissler, Alfred McEwen,

and the HiRISE team for helpful discussions. This work has made use of NASA's Astrophysics Data System, and the USGS Integrated Software for Imagers and Spectrometers (ISIS) [*Gaddis et al.*, 1997; *Eliason et al.*, 2007].

References

Aharonson, O., N. Schorghofer, and M. F. Gerstell (2003), Slope streak formation and dust deposition rates on Mars, *J. Geophys. Res.*, *108*(E12), 5138, doi:10.1029/2003JE002123.

Baratoux, D., et al. (2006), The role of the wind-transported dust in slope streaks activity: Evidence from the HRSC data, *Icarus*, *183*, 30–45.

Beyer, R. A., A. S. McEwen, and R. L. Kirk (2003), Meter-scale slopes of candidate MER landing sites from point photoclinometry, *J. Geophys. Res.*, *108*(E12), 8085, doi:10.1029/2003JE002120.

Cantor, B. A., P. B. James, M. Caplinger, and M. J. Wolff (2001), Martian dust storms: 1999 Mars Orbiter Camera observations, *J. Geophys. Res.*, *106*, 23,653–23,687.

Chuang, F. C., R. A. Beyer, A. S. McEwen, and B. J. Thomson (2007), HiRISE observations of slope streaks on Mars, *Geophys. Res. Lett.*, *34*, L20204, doi:10.1029/2007GL031111.

Eliason, E. M., et al. (2007), HiRISE data processing and standard data products, *Proc. Lunar Planet. Sci. Conf.*, *38*, Abstract 2037.

Ferguson, H. M., and B. K. Lucchitta (1984), Dark streaks on talus slopes, Mars, *NASA Tech. Memo.*, *TM-86246*, 188–190.

Ferris, J. C., J. M. Dohm, V. R. Baker, and T. Maddock III (2002), Dark slope streaks on Mars: Are aqueous processes involved?, *Geophys. Res. Lett.*, *29*(10), 1490, doi:10.1029/2002GL014936.

Gaddis, L., et al. (1997), An overview of the Integrated Software for Imaging Spectrometers (ISIS), *Proc. Lunar Planet. Sci. Conf.*, *28*, 387.

Geissler, P. E. (2005), Three decades of Martian surface changes, *J. Geophys. Res.*, *110*, E02001, doi:10.1029/2004JE002345.

Gerstell, M. F., O. Aharonson, and N. Schorghofer (2004), A distinct class of avalanche scars on Mars, *Icarus*, *168*, 122–130.

Head, J. W., D. R. Marchant, J. L. Dickson, J. S. Levy, and G. A. Morgan (2007), Slope streaks in the Antarctic dry valleys: Characteristics, candidate formation mechanisms, and implications for slope streak formation in the Martian Environment, *Lunar Planet. Sci.*, *XXXVIII*, Abstract 1935.

Malin, M. C., and K. S. Edgett (2001), Mars Global Surveyor Mars Orbiter Camera: Interplanetary cruise through primary mission, *J. Geophys. Res.*, *106*, 23,429–23,570.

Malin, M. C., K. S. Edgett, L. V. Posiolova, S. M. McColley, and E. Z. N. Dobrea (2006), Present-day impact cratering rate and contemporary gully activity on Mars, *Science*, *314*, 1573–1577, doi:10.1126/science.1135156.

McEwen, A. S., et al. (2007), Mars Reconnaissance Orbiter's High Resolution Imaging Science Experiment (HiRISE), *J. Geophys. Res.*, *112*, E05S02, doi:10.1029/2005JE002605.

Miyamoto, H., J. M. Dohm, R. A. Beyer, and V. R. Baker (2004), Fluid dynamical implications of anastomosing slope streaks on Mars, *J. Geophys. Res.*, *109*, E06008, doi:10.1029/2003JE002234.

Morris, E. (1982), Aureole deposits of the Martian volcano Olympus Mons, *J. Geophys. Res.*, *87*, 1164–1178.

Neukum, G., et al. (2004), Recent and episodic volcanic and glacial activity on Mars revealed by the High Resolution Stereo Camera, *Nature*, *432*, 971–979.

Putzig, N. E., M. T. Mellon, K. A. Kretke, and R. E. Arvidson (2005), Global thermal inertia and surface properties of Mars from the MGS mapping mission, *Icarus*, *173*, 325–341.

Rouse, H. (1937), Modern conceptions of the mechanics of turbulence, *Trans. Am. Soc. Civ. Eng.*, *102*, 463–543.

Schorghofer, N., O. Aharonson, and S. Khatiwala (2002), Slope streaks on Mars: Correlations with surface properties and the potential role of water, *Geophys. Res. Lett.*, *29*(23), 2126, doi:10.1029/2002GL015889.

Schorghofer, N., O. Aharonson, M. F. Gerstell, and L. Tatsumi (2007), Three decades of slope streak activity on Mars, *Icarus*, in press.

Scott, D. H., and K. L. Tanaka (1986), Geologic map of the western equatorial region of Mars, *U.S. Geol. Surv. Misc. Geol. Invest. Map*, *I-1802-A.*

Smith, D. E., G. Neumann, P. Ford, R. E. Arvidson, E. A. Guinness, and S. Slavney (1999), Mars Global Surveyor Laser Altimeter Precision Experiment data record, *Rep. MGS-M-MOLA-3-PEDR-L1A-V1.0*, NASA Planet. Data Syst., Greenbelt, Md.

Sullivan, R., P. Thomas, J. Veverka, M. Malin, and K. S. Edgett (2001), Mass movement slope streaks imaged by the Mars Orbiter Camera, *J. Geophys. Res.*, *106*, 23,607–23,633.

Verba, C. A., and C. B. Phillips (2006), Formation of Martian slope streaks: Implications for aqueous processes, *Eos Trans. AGU*, *87*(52), Fall Meet. Suppl., Abstract P34B-05.

Williams, S. H. (1991), Dark talus streaks on Mars are similar to aeolian dark streaks, *Lunar Planet. Sci.*, *XXII*, 1509–1510.

R. A. Beyer, D. M. Burr, and C. B. Phillips, Carl Sagan Center for the Study of Life in the Universe, SETI Institute, 515 N. Whisman Road, Mountain View, CA 94043, USA. (phillips@seti.org)